ACS APPLIED MATERIALS & INTERFACES

Research Article

www.acsami.org

Synthesis and Characterization of PEGylated Polyethylenimine-Entrapped Gold Nanoparticles for Blood Pool and Tumor CT Imaging

Benqing Zhou,[†,∥] Linfeng Zheng,[‡,∥] Chen Peng,[§] Du Li,[§] Jingchao Li,[†] Shihui Wen,[†] Mingwu Shen,*[,†] Guixiang Zhang,*[,‡] and Xiangyang Shi*[,†,§]

[†]College of Chemistry, Chemical Engineering and Biotechnology, Donghua University, Shanghai 201620, People's Republic of China

[‡]Department of Radiology, Shanghai First People's Hospital, Shanghai Jiaotong University, Shanghai 200080, People's Republic of China

[§]State Key Laboratory for Modification of Chemical Fibers and Polymer Materials, College of Materials Science and Engineering, Donghua University, Shanghai 201620, People's Republic of China

Supporting Information

ABSTRACT: The synthesis and characterization of gold nanoparticles (AuNPs) entrapped within polyethylene glycol (PEG)-modified polyethylenimine (PEI) for blood pool and tumor computed tomography (CT) imaging are reported. In this approach, partially PEGylated PEI was used as a template for AuNP synthesis, followed by acetylating the PEI remaining surface amines. The synthesized PEGylated PEI-entrapped AuNPs (Au PENPs) were characterized via different methods. Our results reveal that the synthesized Au PENPs can be tuned to have an Au core size in a range of 1.9−4.6 nm and to be water-soluble, stable, and noncytotoxic in a studied concentration range. With a demonstrated better X-ray attenuation property than that of clinically used iodinated small molecular contrast agent (e.g., Omnipaque) and the prolonged half-decay time (11.2 h in rat) confirmed by pharmacokinetics studies, the developed PEGylated Au PENPs enabled efficient and enhanced blood pool CT imaging with imaging time up to 75 min. Likewise, thanks to the enhanced permeability and retention effect, the PEGylated Au PENPs were also able to be used as a contrast agent for effective CT imaging of a tumor model. With the proven organ biocompatibility by histological studies, the designed PEGylated Au PENPs may hold great promise to be used as contrast agents for CT imaging of a variety of biological systems. The significance of this study is that rather than the use of dendrimers as templates, cost-effective branched polymers (e.g., PEI) can be used as templates to generate functionalized AuNPs for CT imaging applications.

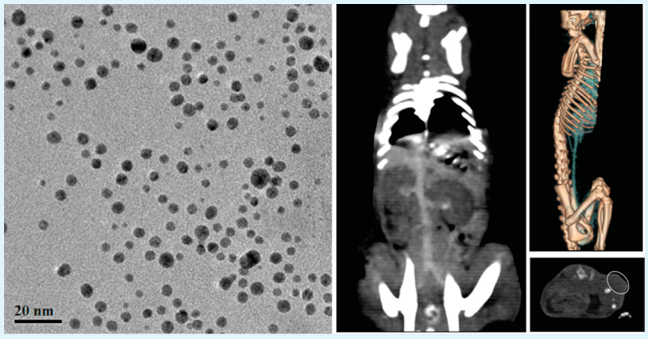

KEYWORDS: *polyethylenimine, gold nanoparticles, PEGylation, blood pool CT imaging, tumors*

INTRODUCTION

Recent progress in nanotechnology has afforded the creation of a variety of nanoparticles (NPs) as imaging probes for biomedical applications.[1−7] For instance, magnetic NPs such as gadolinium-based T_1 contrast agents and superparamagnetic iron oxide-based T_2 contrast agents have been used in magnetic resonance imaging applications;[8−13] quantum dots have been widely studied as fluorescent probes for optical imaging;[14−17] and gold, bismuth sulfide, or tantalum oxide NPs can be used as contrast agents for computed tomography (CT) imaging.[18−21]

CT is one of the most extensively used diagnostic imaging techniques in hospitals due to its merits, including high spatial and density resolution, deep penetration capability, facile post image-processing technique, and cost effectiveness.[22,23] For high-quality CT imaging applications, contrast agents are generally required. Conventional iodine-based small molecular contrast agents (e.g., Omnipaque) display serious shortcomings, such as short imaging time due to the fast elimination by the kidney, nonspecificity, and renal toxicity at a relatively high concentration.[24−26] Due to the possessed advantages of nanoparticulate CT contrast agents such as extended blood circulation time, better X-ray attenuation property than iodinated small molecular CT contrast agents, and good biocompatibility after surface modification, gold NPs (AuNPs) have been paid a great deal of attention.[27]

Among the different polymer-based methods to forming AuNPs,[28−32] dendrimer templating or stabilization strategies have been demonstrated to be powerful to generate dendrimer-entrapped or dendrimer-stabilized AuNPs for CT imaging applications.[7,11,13,33−43] The major advantage of the use of dendrimer nanotechnology is that the functionalization of the particle surfaces can be mediated by modification of dendrimers

Received: July 29, 2014
Accepted: September 11, 2014
Published: September 11, 2014

either before or after the formation of AuNPs. Furthermore, by surface modification with polyethylene glycol (PEG), the dendrimer periphery can be enlarged for more Au entrapment within the dendrimer interiors,[11,13,36,37,40,41,44] allowing for more sensitive CT imaging applications. Likewise, the PEGylation modification of dendrimers renders the formed AuNPs with improved biocompatibility, prolonged blood circulation time, and reduced macrophage cellular uptake, which is beneficial for enhanced blood pool and tumor CT imaging applications.[37,40,41]

Branched polyethylenimine (PEI) displays a structural similarity to dendrimers in terms of the branched internal structure and abundant surface primary amines.[45−48] Importantly, commercially available PEI can be easily prepared using an AB-type monomer via a simple one-step reaction, which is significantly different from the dendrimer synthesis via a time-consuming divergent or convergent technology.[49] The PEI surface amines can be functionalized, followed by synthesis of PEI-entrapped or PEI-stabilized AuNPs.[50−53] In our previous work, we have shown that branched PEI can be used to form AuNPs by either a mild self-reduction chemistry via PEI amines or $NaBH_4$ reduction chemistry.[54−56] These prior successes related to dendrimer nanotechnology and PEI-based chemistry for the synthesis of AuNPs led us to hypothesize that surface-functionalized branched PEI may be used as a template to entrap AuNPs for CT imaging application, thereby providing a unique opportunity to avoid the use of expensive dendrimers.

In the present study, branched PEI was first partially PEGylated via 1-ethyl-3-(3-(dimethylamino)propyl) carbodiimide hydrochloride (EDC) chemistry. The partially PEGylated PEI was used as a template to synthesize AuNPs. This was followed by acetylating the remaining PEI surface amines (Scheme 1). The synthesized PEGylated PEI-entrapped AuNPs (Au PENPs) were well characterized through various technologies. The cytocompatibility and hemocompatibility of the particles were tested by cell morphology observation, cell viability assay, and hemolytic assay. Pharmacokinetic studies were carried out by inductively coupled plasma-optical emission spectroscopy (ICP-OES) to evaluate the half-decay time of the PEGylated Au PENPs. Lastly, the synthesized PEGylated Au PENPs were used for both blood pool CT imaging of rats and in vivo CT imaging of a xenografted tumor model of mice. To the best of our knowledge, this is the first report associated with the synthesis of PEGylated Au PENPs for CT imaging applications.

Scheme 1. Schematic Illustration of the Preparation of PEGylated Au PENPs for CT Imaging Applications.[a]

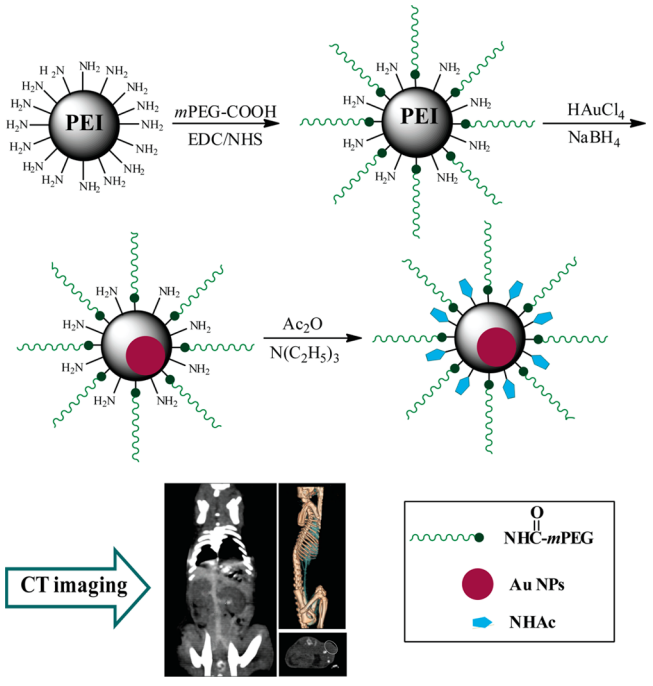

[a]Ac_2O and $N(C_2H_5)_3$ represents acetic anhydride and triethylamine, respectively.

EXPERIMENTAL SECTION

Materials. Branched PEI (average molecular weight, M_w = 25 000) was purchased from Aldrich (St. Louis, MO). PEG monomethyl ether with a carboxyl end group (*m*PEG-COOH, M_w = 2000) was from Shanghai Yanyi Biotechnology Corporation (Shanghai, China). EDC and *N*-hydroxysuccinimide (NHS) were from J&K Chemical, Ltd. (Shanghai, China). Acetic anhydride, triethylamine, $HAuCl_4{\cdot}4H_2O$, and all other chemicals were obtained from Sinopharm Chemical Reagent Co., Ltd. (Shanghai, China). 3-(4,5-Dimethylthiazol-2-yl)-2,5-diphenyltetrazolium bromide (MTT) was acquired from Shanghai Sangon Biological Engineering Technology & Services Co., Ltd. (Shanghai, China). KB cells, a human epithelial carcinoma cell line, were supplied from the Institute of Biochemistry and Cell Biology, the Chinese Academy of Sciences (Shanghai, China). RPMI-1640 medium, fetal bovine serum (FBS), penicillin, and streptomycin were from Hangzhou Jinuo Biomedical Technology (Hangzhou, China). All chemicals and materials were used as received. Water used in all experiments was treated using a Milli-Q Plus 185 water purification system (Millipore, Bedford, MA) to have a resistivity higher than 18.2 MΩ·cm. Regenerated cellulose dialysis membranes having a molecular weight cutoff (MWCO) of 14 000 were purchased from Fisher (Pittsburgh, PA).

Synthesis of PEGylated Au PENPs. *m*PEG-COOH (60.0 mg, 0.03 mmol, 5.0 mL in water) was activated by EDC/NHS (10 mol equiv of *m*PEG-COOH, 57.5 mg EDC and 34.5 mg NHS) under magnetic stirring for 3 h at room temperature. The activated *m*PEG-COOH was then dropped into a PEI solution (25.0 mg, 0.001 mmol, 10.0 mL in water) under magnetic stirring at room temperature. The reaction mixture was continuously stirred for 3 days to complete the reaction. Then the reaction mixture solution was extensively dialyzed against phosphate buffered saline (PBS, three times, 2 L) and water (six times, 2 L) using a dialysis membrane with an MWCO of 14 000 for 3 days, followed by a freeze-drying process to obtain the PEI·NH_2-*m*PEG product.

PEGylated Au PENPs were synthesized according to protocols described in the literature.[34,41] $NaBH_4$ reduction chemistry was used to prepare PEGylated Au PENPs with Au salt/PEI·NH_2-*m*PEG molar ratios of 50:1, 100:1, 150:1, 200:1, 250:1, 300:1, 350:1, and 400:1, respectively. Using the Au salt/PEI·NH_2-*m*PEG molar ratio at 200:1 as an example, a certain amount of $HAuCl_4$ solution (10 mg/mL in water) was dropped into a water solution of PEI·NH_2-*m*PEG (25 mg, 100 mL) under vigorous magnetic stirring. Thirty minutes later, $NaBH_4$ solution (5 mL in water) pretreated with a water/ice mixture having 5 mol equiv to the Au salt was rapidly added into the Au salt/PEI·NH_2-*m*PEG mixture solution under stirring. Within a few seconds, the reaction mixture turned deep red. The reaction mixture was continuously stirred for 3 h. The finally formed PEGylated Au PENPs were denoted as [$(Au^0)_n$-PEI·NH_2-*m*PEG] (n = 50, 100, 150, 200, 250, 300, 350, and 400, respectively).

The formed [$(Au^0)_n$-PEI·NH_2-*m*PEG] NPs were subjected to acetylation to modify the remaining PEI surface amines according to protocols reported in the literature.[57,58] Briefly, triethylamine (92.0 μL) was dropped into a water solution of [$(Au^0)_n$-PEI·NH_2-*m*PEG] NPs (the mass of PEI·NH_2-*m*PEG was 25 mg in 100 mL water) under vigorous magnetic stirring for 30 min. Acetic anhydride (76.6 μL) with

5 mol equiv to the remaining PEI primary amines was then added to the above mixture solution, and the mixture was reacted for 24 h. The reaction mixture was then completely dialyzed against PBS (three times, 2 L) and water (six times, 2 L) for 3 days using a dialysis membrane with an MWCO of 14 000. This was followed by a freeze-drying process to get the $[(Au^0)_n$-PEI·NHAc-*m*PEG] NPs.

Characterization Techniques. ^{1}H NMR spectra were collected on a Bruker DRX 400 nuclear magnetic resonance spectrometer. D_2O was used as a solvent to dissolve all samples before experiments. Matrix-assisted laser desorption ionization-time-of-flight (MALDI-TOF) mass spectra were recorded using a 4800 Plus MALDI-TOF/TOF Analyzer (AB SCIEX, Framingham, MA). We selected linear mode as the operation mode. Beta-indoleacrylic acid dissolved in acetonitrile/H_2O (10 mg/mL, v/v = 70:30) was used as the matrix, and the sample (1 mg) was dissolved in 1 mL methanol. Equal volumes of the sample solution and the matrix solution were well mixed. Then, the mixture solution with a volume of 1 μL was injected onto the spot of the target plate before measurements. UV−vis spectroscopy was carried out using a Lambda 25 UV−vis spectrophotometer (PerkinElmer, Boston, MA). Before the experiments, all samples were dissolved in water. A JEOL 2010F analytical electron microscope (JEOL, Tokyo, Japan) was used to characterize the size and morphology of the samples at an operating voltage of 200 kV via transmission electron microscopy (TEM) imaging. TEM samples were prepared by dropping an aqueous particle suspension (1 mg/mL) onto a carbon-coated copper grid, and the aqueous suspension was air-dried before measurements. Zeta potential and dynamic light scattering (DLS) were tested using a Malvern Zetasizer Nano ZS model ZEN3600 (Worcestershire, U.K.) coupled with a standard laser with a wavelength of 633 nm. Thermogravimetric analysis (TGA) was carried out on a TG209F1 system (Netzsch, Germany) under air atmosphere at a heating rate of 20 °C/min.

Cell Culture. KB cells were regularly cultured and passaged in RPMI-1640 medium containing 10% FBS, 100 U/mL penicillin, and 100 μg/mL streptomycin at 37 °C and 5% CO_2.

Cytotoxicity Assay. The cytotoxicity of the PEGylated Au PENPs was measured by a standard MTT assay method. Briefly, 1×10^4 KB cells were seeded in each well of a 96-well plate with 200 μL RPMI-1640 medium. After overnight culture to make the cells well attached, the medium was substituted with fresh medium containing $[(Au^0)_{200}$-PEI·NHAc-*m*PEG] NPs with different concentrations (0−300 μg/mL). The cells were then incubated at 37 °C and 5% CO_2 for 24 h. Then, MTT (20 μL, 5 mg/mL) in PBS was added to each well and the cells were incubated for another 4 h. The assays were performed according to the manufacturer's instructions. The absorbance at 570 nm in each well was recorded by a Thermo Scientific Multiskan MK3 ELISA reader (Thermo Scientific, Waltham, MA). Triplicate wells for each sample were recorded to calculate the mean and standard deviation.

Likewise, after the cells were treated with $[(Au^0)_{200}$-PEI·NHAc-*m*PEG] NPs at different concentrations (0−300 μg/mL) for 24 h, the morphology of the KB cells was visualized using a Leica DM IL LED inverted phase contrast microscope (Wetzlar, Germany) at a magnification of 100× for each sample.

Hemolysis Assay. Fresh heparin-stabilized human blood was supplied from Shanghai First People's Hospital (Shanghai, China) and used with approval by the Ethical Committee of Shanghai First People's Hospital. Human red blood cells (HRBCs) were isolated, purified, and used to test the hemolysis effect of PEGylated Au PENPs according to protocols described in our previous work.[7,56] In order to subtract the contribution of the surface plasma band of Au PENPs, we also recorded the absorption of Au PENPs at 577 nm before incubation with HRBCs as the blank control by UV−vis spectrometry. The hemoglobin was determined at 577 nm in all measurements.

X-ray Attenuation Measurements. Aqueous solutions of the $[(Au^0)_{200}$-PEI·NHAc-*m*PEG] NPs (0.1 mL) with different Au concentrations and iohexol 300 (Omnipaque 300 mg I/mL, GE Healthcare) with different iodine concentrations (0.1 mL) were prepared in 2.0 mL-Eppendorf tubes and placed in a homemade scanning holder. CT scanning was carried out according to procedures and instrumental conditions reported in our previous work[41] using a GE Light Speed VCT imaging system (GE Medical System).

Pharmacokinetics. All animal experiments were carried out following the protocols approved by the Ethical Committee of Shanghai First People's Hospital and the policy of the National Ministry of Health. Female Sprague−Dawley (SD) rats (150−200 g) were purchased from the Shanghai SLAC Laboratory Animal Center (Shanghai, China). Each rat was intravenously injected with a PBS solution containing $[(Au^0)_{200}$-PEI·NHAc-*m*PEG] NPs ([Au] = 0.1 M, 500 μL) through the tail vein. The blood sample at each time point postinjection was collected. The Au concentration in the blood samples was quantified using a Leeman Prodigy ICP-OES system (Hudson, NH). The half-decay time ($t_{1/2}$) of Au concentration was analyzed according to the method reported in our previous work.[41]

Blood Pool CT Imaging. Healthy adult SD rats (150−200 g, Shanghai SLAC Laboratory Animal Center) were anesthetized by intraperitoneal injection of pentobarbital sodium (40 mg/kg). Then a PBS solution of $[(Au^0)_{200}$-PEI·NHAc-*m*PEG] NPs ([Au] = 0.1 M, 800 μL) was intravenously injected into each rat through the tail vein. The rat was placed in a scanning holder and CT scanning was performed using GE Light Speed VCT imaging system at 0.5, 30, and 75 min postinjection, respectively, using instrumental parameters similar to those reported in our previous work.[41]

In Vivo CT Imaging of Xenografted KB Tumor Model. Male 4- to 6-week-old BALB/c nude mice (15−20 g) provided by Shanghai SLAC Laboratory Animal Center were subcutaneously injected with 1.5×10^6 KB cells/mouse on the right side of their flanks. When the tumor grew to a volume of 0.5−1.2 cm^3, around 3 weeks postinjection, the mice were intraperitoneally injected with pentobarbital sodium (40 mg/kg) to be anesthetized. Then, $[(Au^0)_{200}$-PEI·NHAc-*m*PEG] NPs ([Au] = 0.1 M, 150 μL in PBS) were intravenously delivered to each mouse via the tail vein. CT scanning was performed according to the procedures similar to the blood pool CT imaging of rats before and at 1, 1.5, 2.5, 3.5, and 5 h postinjection.

Silver Staining. After CT scanning, the tumor-bearing nude mice were killed to extract the tumors. The tumors were then fixed, dehydrated, embedded with paraffin, and sectioned for silver staining, following protocols described in the literature.[40] The silver-stained sections were dried in air, dehydrated, and mounted on coverslips before optical microscopic observation. The tumor sections from the tumor-bearing nude mice without injection of the PEGylated Au PENPs were also silver stained for comparison.

In Vivo Biodistribution of PEGylated Au PENPs. The C57BL/6 mice (20−25 g, Shanghai SLAC Laboratory Animal Center) were anesthetized by intraperitoneal injection of pentobarbital sodium (40 mg/kg). Then, after intravenous injection of $[(Au^0)_{200}$-PEI·NHAc-*m*PEG] NPs ([Au] = 0.1 M, 100 μL in PBS) through the tail vein for each mouse, the mice were sacrificed at different time points postinjection (0, 1, 4, 12, 24, and 48 h, respectively), and the heart, lung, stomach, spleen, liver, intestines, kidney, brain, and blood were extracted and weighed. The organs were treated in aqua regia solution overnight. The Au content in different organs was subsequently analyzed by ICP-OES.

Histological Evaluation of the Organ Toxicity. To evaluate the long-term organ toxicity of PEGylated Au PENPs in vivo, C57BL/6 mice were intravenously administered $[(Au^0)_{200}$-PEI·NHAc-*m*PEG] NPs ([Au] = 0.1 M, 100 μL in PBS, for each mouse). PBS (100 μL) was used as control. After one month, the mice were anesthetized, and the liver, lung, spleen, heart, and kidney were harvested, washed with PBS, and immediately fixed with 4% buffered formalin solution. After 24 h fixation, the organs were processed, sectioned, and hematoxylin and eosin (H&E) stained for optical microscopic observation according to standard protocols reported in the literature.[40]

Statistical Analysis. Statistical analysis was performed via standard ANOVA statistical method described in our previous work.[11]

RESULTS AND DISCUSSION

Synthesis and Characterization of PEGylated Au PENPs. Similar to our previous study related to the use of

PEGylated generation 5 (G5) poly(amidoamine) (PAMAM) dendrimers as templates to synthesize AuNPs,[41] in this work, PEI was first PEGylated, and then used as a template to generate AuNPs. This was followed by acetylating the remaining PEI surface amines using acetic anhydride. The prepared PEGylated Au PENPs were used as contrast agents for CT imaging applications (Scheme 1).

Various techniques were employed to characterize the synthesized PEGylated Au PENPs. First, the formed PEI·NH_2-*m*PEG conjugate was characterized by ^{1}H NMR (Figure S1a, Supporting Information). It is clear that the peaks at 2.4−3.5 ppm can be assigned to the $-CH_2-$ proton signals of PEI, while the peaks at 3.5−3.8 ppm are associated with the $-CH_2-$ protons of PEG.[45,50,59] On the basis of the comparison of the NMR integration, each PEI was estimated to have 26 *m*PEG moieties linked. This number is very close to the initial molar feeding ratio (*m*PEG-COOH/PEI = 30:1). Further MALDI-TOF mass spectral analysis of the formed PEI·NH_2-*m*PEG conjugate reveals that the M_w of the PEI·NH_2-*m*PEG conjugate is 76 982.2 (Figure S2, Supporting Information). By subtracting the average M_w of the PEI (25 000), the number of *m*PEG moieties attached to each PEI was calculated to be 26, corroborating the ^{1}H NMR data.

The formed PEI·NH_2-*m*PEG conjugates were then employed as templates to form AuNPs using $NaBH_4$ as a reducing agent. This was followed by acetylating the remaining PEI surface amines using acetic anhydride. By varying the initial Au salt/PEI·NH_2-*m*PEG molar ratio, the [$(Au^0)_n$-PEI·NHAc-*m*PEG] NPs with different Au compositions were formed. ^{1}H NMR was used to confirm the successful acetylation reaction (Figure S1b, Supporting Information). For instance, [$(Au^0)_{200}$-PEI·NHAc-*m*PEG] NPs display two new proton peaks at 1.8 and 2.1 ppm, respectively. The peak at 1.8 ppm is associated with the acetyl protons linked with the secondary amides, whereas the peak at 2.1 ppm is assigned to the acetyl protons linked with the tertiary amides, in agreement with the literature.[50] Zeta-potential measurements were also carried out to confirm the surface potential changes after the acetylation reaction. The positive potential of the [$(Au^0)_{200}$-PEI·NH_2-*m*PEG] NPs (29.77 ± 8.59 mV) significantly decreased after the acetylation to form the [$(Au^0)_{200}$-PEI·NHAc-*m*PEG] NPs (8.55 ± 1.80 mV). The slightly positive charge of the [$(Au^0)_{200}$-PEI·NHAc-*m*PEG] NPs may be attributed to the fact that a portion of the PEI amines required to stabilize the AuNPs is unable to be acetylated, similar to our previous results associated with dendrimer-entrapped AuNPs (Au DENPs).[57] Our experimental data suggest that the entrapment of AuNPs within the partially PEGylated PEI does not compromise the transformation of PEI amines to acetyl groups.

The formation of AuNPs before and after acetylation of the PEI remaining surface amines was first confirmed by visualization of the wine red color of the solutions at a concentration of 0.1 mg/mL (Figure 1, insets). It is clear that the wine red color of these PEGylated Au PENPs becomes deeper and deeper with the Au salt/PEI-*m*PEG molar ratio, in agreement with our previous reports.[34,41] UV−vis spectra data reveal that all the PEGylated Au PENPs exhibit a typical surface plasmon resonance (SPR) peak at 520 nm (Figure 1) with a higher SPR peak intensity at a higher Au salt/PEI-*m*PEG molar ratio, demonstrating the successful formation of AuNPs.[60,61] Our results also suggest that acetylation of the remaining PEI surface amines does not significantly impact the optical property of the Au PENPs.

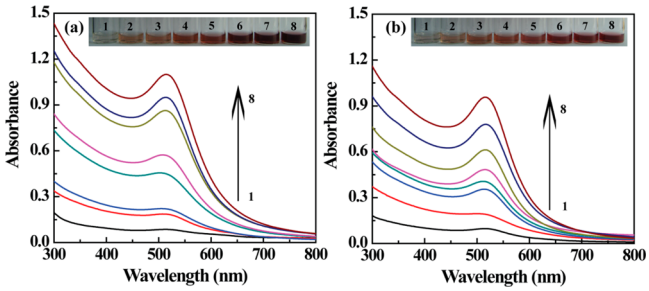

Figure 1. UV−vis spectra of the (a) [$(Au^0)_n$-PEI·NH_2-*m*PEG] and (b) [$(Au^0)_n$-PEI·NHAc-*m*PEG] NPs, and (insets) photographs of the respective suspensions of the Au PENPs (0.1 mg/mL); *n* = (1) 50, (2) 100, (3) 150, (4) 200, (5) 250, (6) 300, (7) 350, and (8) 400.

The size and morphology of the formed [$(Au^0)_n$-PEI·NHAc-*m*PEG] NPs were characterized by TEM (Figure 2). It can be seen that the size of PEGylated Au PENPs at a given Au salt/

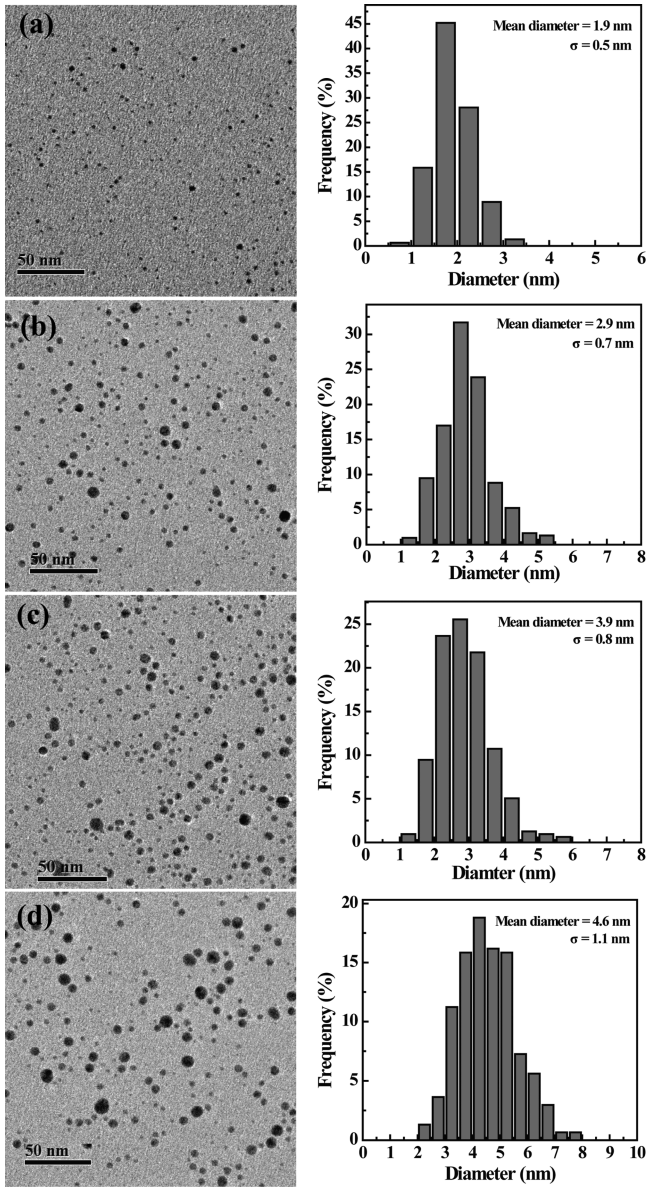

Figure 2. TEM images and size distribution histograms of the [$(Au^0)_n$-PEI·NHAc-*m*PEG] NPs (*n* = (a) 100, (b) 200, (c) 300, and (d) 400).

PEI-*m*PEG molar ratio is small and quite uniform. By changing the Au salt/PEI-*m*PEG molar ratio, the size of the PEGylated Au PENPs can be tuned from 1.9 to 4.6 nm. At the Au salt/PEI-*m*PEG molar ratio of 400:1, the mean size of the Au core NPs is still less than 5 nm. This suggests that partially PEGylated PEI can be used as a template to effectively restrict the growth of AuNPs, quite similar to the PEGylated G5 dendrimer templates used to synthesize AuNPs.[41] For comparison, primary PEI without PEGylation was also used to synthesize AuNPs under similar experimental conditions (Figure S3, Supporting Information). We show that at the Au salt/PEI molar ratios of 100:1 and 150:1, the formed AuNPs are quite stable (Figure S3a, Supporting Information); however, after acetylation of the PEI surface amines, the AuNPs start to have a certain degree of aggregation and precipitation (Figure S3b, Supporting Information). This implies that partial PEGylation of PEI surface amines is able to render the formation of stable Au PENPs with a quite high Au salt/PEI molar ratio even after the PEI remaining surface amines are acetylated, which is essential for CT imaging applications with a high sensitivity. It should be noted that branched PEI (M_w = 25 000) has a size comparable to that of G5 PAMAM dendrimers (M_w = 28 826), and the surface PEGylation of PEI enables effective entrapment of AuNPs, similar to PEGylated G5 dendrimers reported in our previous study.[41] Negatively stained TEM image of $[(Au^0)_{350}$-PEI·NHAc-*m*PEG] NPs clearly shows that each AuNP is surrounded with a white ring associated with the PEGylated PEI, indicating the effective entrapment of AuNPs within the PEGylated PEI polymers (Figure S4, Supporting Information).

High-resolution TEM was used to characterize the crystalline structure of PEGylated Au PENPs (Figure S5a, Supporting Information). Lattices of Au crystals can be clearly observed, confirming the crystalline structure of the Au core NPs. The crystalline structure of Au core NPs was further validated by selected area electron diffraction (SAED), where the (111), (200), (220), and (311) rings are typical features of the face-centered-cubic (fcc) crystal structure (Figure S5b, Supporting Information). Energy dispersive spectroscopy (EDS) analysis of the PEGylated Au PENPs confirmed the presence of gold element (Figure S5c, Supporting Information). The hydrodynamic sizes of the PEGylated Au PENPs before and after acetylation were measured using DLS (Table S1, Supporting Information). The hydrodynamic sizes of all Au PENPs, regardless of the acetylation modification, range from 110 to 290 nm. The size of Au PENPs at a given Au salt/PEI-*m*PEG molar ratio is much larger than that determined by TEM. This may be due to the fact that DLS measures the particles in a clustered state in aqueous solution, which is likely to consist of many single Au PENPs, while TEM only measures the size of single Au core NPs.

The composition of Au loaded within the PEGylated PEI was quantified by TGA (Figure S6, Supporting Information). For instance, by subtracting the remaining weight of PEI·NHAc-*m*PEG (6.72%) from $[(Au^0)_{200}$-PEI·NHAc-*m*PEG] NPs (35.31%) at a temperature of 900 °C, the number of Au atom per PEI was calculated to be 199, approximately similar to the Au salt/PEI-*m*PEG molar feeding ratio of 200:1. This suggests that all the added Au salt has been thoroughly reduced by $NaBH_4$.

Stability of PEGylated Au PENPs. The stability of PEGylated Au PENPs is important for their further biomedical applications. Similar to our previous study related to Au DENPs,[34,40,41] UV−vis spectroscopy was used to assess the stability of the PEGylated Au PENPs under different pH and temperature conditions (Figures S7 and S8, Supporting Information). We show that the PEGylated Au PENPs dispersed in water at different pHs (pH = 5, 6, 7, and 8) and temperatures (4, 25, 37, and 50 °C) do not display obvious changes in the absorption features, especially the SPR bands of AuNPs. Furthermore, the PEGylated Au PENPs dispersed in water, PBS, and cell culture medium are stable and do not have any apparent aggregation and precipitation, even after being stored for one month at room temperature. The good colloidal stability of the PEGylated Au PENPs is prerequisite for their further biomedical imaging applications. For simplicity, we selected $[(Au^0)_{200}$-PEI·NHAc-*m*PEG] NPs as a model NP system to test their biocompatibility and CT imaging performances in vitro and in vivo.

Hemolytic Assay. Hemocompatibility is vital for nanoparticulate contrast agents to be used in vivo, especially under a certain circumstance that needs the NPs to contact blood. Hemolytic assay of the $[(Au^0)_{200}$-PEI·NHAc-*m*PEG] NPs was executed according to our previous reports.[7,21] The hemolytic behaviors of the $[(Au^0)_{200}$-PEI·NHAc-*m*PEG] NPs at different concentrations reveal that the $[(Au^0)_{200}$-PEI·NHAc-*m*PEG] NPs do not exhibit any apparent hemolytic effect in a concentration range of 0−400 μg/mL (Figure S9, Supporting Information). This is significantly different from the positive control (water). Further quantitative analysis shows that the hemolysis percentages of the $[(Au^0)_{200}$-PEI·NHAc-*m*PEG] NPs in the studied concentration range of 50−400 μg/mL are all less than 5% (Figure S9c, Supporting Information), demonstrating the excellent hemocompatibility of the PEGylated Au PENPs.

Cytotoxicity Assay. We next assessed the cytotoxicity of the $[(Au^0)_{200}$-PEI·NHAc-*m*PEG] NPs. The cytotoxicity of the $[(Au^0)_{200}$-PEI·NHAc-*m*PEG] NPs was tested via MTT viability assay of KB cells incubated with the particles at different concentrations (Figure 3a). It is clear that cells treated with the

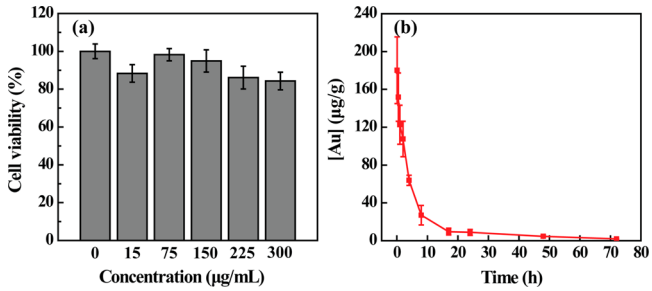

Figure 3. (a) MTT viability assay of KB cells after treatment with the $[(Au^0)_{200}$-PEI·NHAc-*m*PEG] NPs at different concentrations for 24 h; (b) blood circulation and pharmacokinetic data obtained for the $[(Au^0)_{200}$-PEI·NHAc-*m*PEG] NPs ([Au] = 0.1 M, 500 μL in PBS, for each rat) in healthy rats (n = 3).

$[(Au^0)_{200}$-PEI·NHAc-*m*PEG] NPs in a concentration range of 0−300 μg/mL have approximately similar viability to the PBS control ($p > 0.05$, n = 3). This suggests that the $[(Au^0)_{200}$-PEI·NHAc-*m*PEG] NPs do not display apparent cytotoxicity in the studied concentration range.

The cytotoxicity of the $[(Au^0)_{200}$-PEI·NHAc-*m*PEG] NPs was further proven via visualization of the morphology of KB cells treated with the particles at different concentrations (Figure S10, Supporting Information). We show that the cells

do not display any apparent morphological variations at the particle concentration up to 300 μg/mL in comparison to the control cells treated with PBS, corroborating the MTT assay data.

Pharmacokinetics. For efficient molecular CT imaging in vivo, it is critical to investigate the pharmacokinetics of the PEGylated Au PENPs. ICP-OES was used to analyze the Au concentration in the blood samples of rats at different time points post intravenous injection of the [$(Au^0)_{200}$-PEI·NHAc-*m*PEG] NPs (Figure 3b). The half-decay time ($t_{1/2}$) was estimated to be 11.2 h, which is comparable to that of PEGylated Au nanorods (12.5 h) reported in the literature,[62] but shorter than PEGylated Au DENPs (31.76 h) reported in our previous work.[41] This implies that the PEGylated Au PENPs have sufficiently long retention time in the blood, which is essential for their applications in both blood pool CT imaging and tumor CT imaging.

X-ray Attenuation Property. Owing to the higher atomic number of Au than that of iodine, AuNPs is expected to have a better X-ray attenuation property than iodinated small molecular CT contrast agents (e.g., Omnipaque). The X-ray attenuation intensity of the [$(Au^0)_{200}$-PEI·NHAc-*m*PEG] NPs was compared with Omnipaque at the same molar concentration of Au or iodine (Figure 4). Note that the Au molar

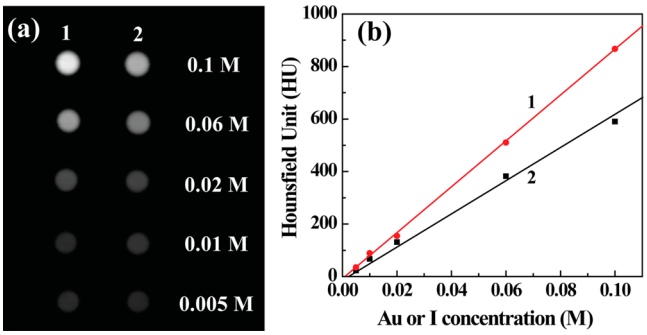

Figure 4. (a) CT images in vitro and (b) X-ray attenuation intensity of the [$(Au^0)_{200}$-PEI·NHAc-*m*PEG] NPs (1) and Omnipaque (2) as a function of the molar concentration of the radiodense element (Au or iodine).

concentration can be calculated based on the estimated M_w of the [$(Au^0)_{200}$-PEI·NHAc-*m*PEG] NPs (1.40×10^5) according to the formula. It can be seen that with the concentration of Au or iodine increased, both [$(Au^0)_{200}$-PEI·NHAc-*m*PEG] NPs and Omnipaque display brighter CT images; however, the brightness of the [$(Au^0)_{200}$-PEI·NHAc-*m*PEG] NPs is more prominent than that of Omnipaque at the same concentration of radiodense element, especially at the higher concentrations (Figure 4a). Quantitative CT value measurements show that the X-ray attenuation intensity of both [$(Au^0)_{200}$-PEI·NHAc-*m*PEG] NPs and Omnipaque increases with the increase of Au or iodine concentration; however, the increasing trend of the [$(Au^0)_{200}$-PEI·NHAc-*m*PEG] NPs is much more significant than that of Omnipaque (Figure 4b). Our results imply that the PEGylated Au PENPs have a better X-ray attenuation property than conventionally used iodinated CT contrast agent, Omnipaque, similar to our previous work related to PEGylated Au DENPs.[37,41]

Application of PEGylated Au PENPs for Blood Pool CT Imaging. We next explored the potential utility of PEGylated Au PENPs as a contrast agent for blood pool CT imaging. [$(Au^0)_{200}$-PEI·NHAc-*m*PEG] NPs dispersed in PBS solution ([Au] = 0.1 M, 800 μL) were intravenously delivered to a rat through the tail vein, and the rat was scanned by a clinical CT imaging system. In general, the rat's blood vessels and other soft tissues such as muscles and connective tissues cannot be differentiated from each other, and only the bones appear to be white due to their stronger X-ray absorption property. The injection of the [$(Au^0)_{200}$-PEI·NHAc-*m*PEG] NPs led to the CT contrast enhancement of different blood vessels and the liver (Figure 5a). The rat's inferior vena cava, left renal vein,

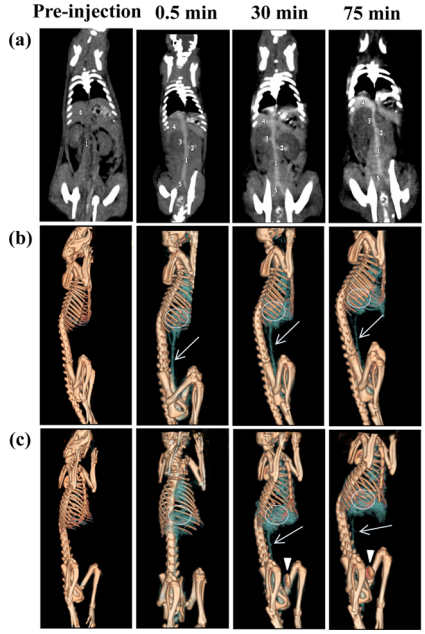

Figure 5. In vivo X-ray CT imaging. (a) Serial CT coronal views of rat's (1) inferior vena cava, (2) left renal vein, (3) right renal vein, (4) liver, (5) and common iliac vein. Corresponding 3D renderings of in vivo CT images at (b) lateral position and (c) lateral oblique position of the rat before injection and at different time points postinjection of [$(Au^0)_{200}$–PEI·NHAc–*m*PEG] ([Au] = 0.1 M, 800 μL in PBS).

right renal vein, liver, and common iliac vein, indicated by 1–5, respectively, can be clearly seen at 0.5 min postinjection, whereas the same blood vessels or organs are not able to be clearly differentiated before injection. This CT contrast enhancement can last until 75 min postinjection. Interestingly, the liver region appeared to be brighter with time postinjection (Figure 5a), which is due to the accumulation of the PEGylated Au PENPs in the liver region. At 75 min postinjection, the vessels of the inferior vena cava, renal vein, and common iliac vein became slightly vaguer than before (Figure 5a). Quantitative analysis of the CT values of liver and the inferior vena cava shows that the liver region has increased CT contrast enhancement with time postinjection, while the CT value of the inferior vena cava reaches the highest at 0.5 min postinjection and slightly decreases with time (Table 1). The CT imaging performance of [$(Au^0)_{200}$–PEI·NHAc–*m*PEG] NPs was further confirmed by the reconstructed 3D CT images, where the liver (white circle) and inferior vena cava (white arrow) regions can be clearly observed (Figure 5b,c). In addition, it seems that the [$(Au^0)_{200}$–PEI·NHAc–*m*PEG] NPs are able to be metabolized via renal filtration, as the bladder region (white arrowhead) has increased CT contrast enhancement at 30 and 75 min postinjection (Figure 5b,c). This is consistent with our

Table 1. Quantitative Analysis of the CT Values in Liver and Inferior Vena Cava at Different Time Points (Mean ± S.D., n = 3)

	CT value (HU)			
		time postinjection		
organ	before injection	0.5 min	30 min	75 min
liver	61.97 ± 2.09	75.67 ± 2.52[a]	84.67 ± 0.58[a]	96.00 ± 1.00[a]
inferior vena cava	62.44 ± 2.01	110.67 ± 3.06[a]	96.00 ± 2.00[a]	86.00 ± 1.00[a]

[a] $P < 0.05$ compared with data before injection.

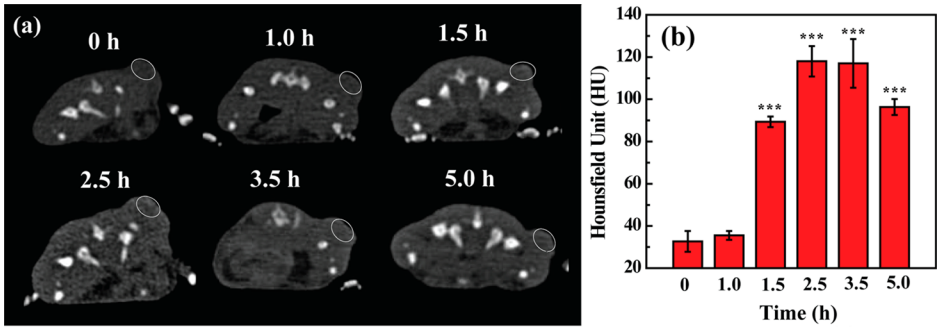

Figure 6. In vivo (a) CT images and (b) CT values of the KB tumor in nude mice before (0 h) and at different time points post intravenous injection of the [$(Au^0)_{200}$-PEI·NHAc-mPEG] NPs ([Au] = 0.1 M, 150 μL in PBS). In panel b, statistical analysis was performed and all data were compared with the one before injection.

previous report.[37] Notably, the rats injected with the [$(Au^0)_{200}$−PEI·NHAc−mPEG] NPs behaved normally as those without treatment and we did not observe any undesirable side effect in rats at 3 weeks postinjection. This suggests that the injected PEGylated Au PENPs do not display in vivo toxicity to the animals.

CT Imaging of Xenografted KB Tumor Model in Vivo. The excellent blood pool CT imaging performance of PEGylated Au PENPs along with their good biocompatibility drove us to pursue their applicability for in vivo CT imaging of a xenografted tumor model in BALB/c nude mice. After intravenous administration of the [$(Au^0)_{200}$-PEI·NHAc-mPEG] NPs via the tail vein, the tumor-bearing mice were scanned by a clinical CT imaging system at different time points (Figure 6). Tumor CT images reveal that the tumor region has a CT contrast enhancement with the time postinjection when compared with that before injection (Figure 6a). Quantitative analysis of the tumor CT values at different time points shows that at 2.5 h postinjection, the CT value of the tumor area is the highest with a tumor ΔCT value (difference in CT values before injection and at 2.5 h post intravenous injection) of 85.3 HU, and even at 5 h postinjection, the tumor CT value is still significantly higher than that before injection (Figure 6b, $p < 0.001$). Compared with PEGylated Au DENPs that can lead to a maximum tumor ΔCT value of 19.5 HU at 6 h post intravenous injection in our previous work,[41] the performance of tumor CT imaging using PEGylated Au PENPs is much better, although the injected Au dose for PEGylated Au DENPs ([Au] = 0.1 M, 100 μL) is less than that for PEGylated Au PENPs ([Au] = 0.1 M, 150 μL). Our results suggest that PEGylated Au PENPs are able to be transported to the tumor site via a passive enhanced permeability and retention (EPR) effect,[63,64] allowing for effective tumor CT imaging, similar to PEGylated Au DENPs described in our previous work.[13,37,41]

To further confirm the tumor uptake of the PEGylated Au PENPs, the tumor-bearing mice were sacrificed to extract the tumors. The tumors were then sectioned for silver staining treatment (Figure S11, Supporting Information). It is obvious that the tumor sections treated with Au PENPs display numerous dark brown spots (Figure S11b, Supporting Information), which are associated with the accumulated Au PENPs in the tumor tissue. In sharp contrast, the negative control tumor section without injection of the PEGylated Au PENPs did not display apparent brown spots. The silver staining results further suggest that the intravenously injected PEGylated Au PENPs are able to be taken up in the tumor area via a passive EPR effect, thereby enabling efficient CT imaging of the tumors in vivo.

In Vivo Biodistribution of PEGylated Au PENPs. For in vivo CT imaging applications, it is crucial to investigate the biodistribution of the PEGylated Au PENPs. At different time points post intravenous injection of the [$(Au^0)_{200}$-PEI·NHAc-mPEG] NPs, the Au uptake in the major organs of the mice including the heart, lung, stomach, spleen, liver, intestine, kidney, brain, and blood was analyzed by ICP-OES (Figure 7). It is clear that the PEGylated Au PENPs are mainly taken up by the liver and spleen (Au concentration is up to 1464.1 and

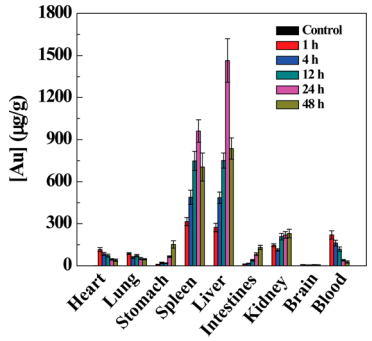

Figure 7. Biodistribution of Au element in the major organs of the mice including the heart, lung, stomach, spleen, liver, intestines, kidney, brain, and blood. The data were recorded from the whole organ taken at different time points post intravenous injection of the [$(Au^0)_{200}$-PEI·NHAc-mPEG] NPs ([Au] = 0.1 M, 100 μL in PBS).

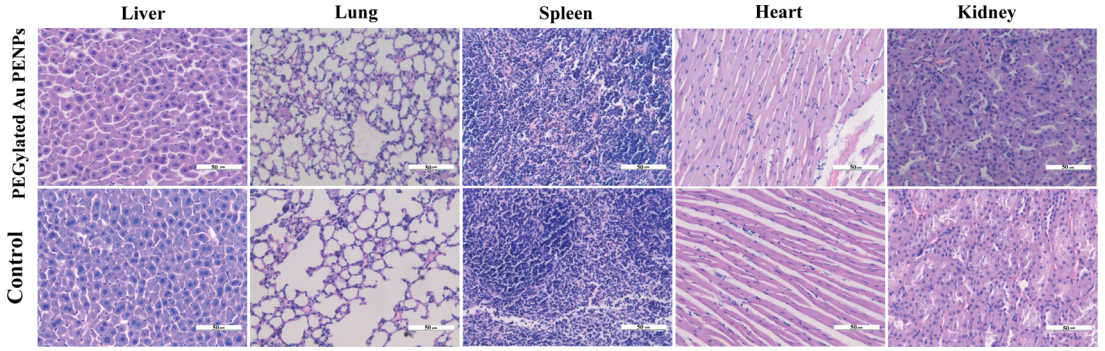

Figure 8. Histological changes in the liver, lung, spleen, heart, and kidney of the mice at 1 month post intravenous injection of the $[(Au^0)_{200}$-PEI·NHAc-*m*PEG] NPs ([Au] = 0.1 M, 100 μL in PBS). Mice injected with 100 μL PBS were used as control. These organ sections were H&E stained and observed under a optical microscope at 200× magnification (the scale bar in each panel indicates 50 μm).

960.9 μg/g at 24 h postinjection, respectively) and start to decrease at 48 h postinjection. The Au concentration in blood decreases gradually from 220.3 to 26.7 μg/g at 1−48 h postinjection. Our data show that the PEGylated Au PENPs can be eliminated from blood, taken up by the liver and spleen, and then accumulated in kidney. This also implies that PEGylated Au PENPs are able to evade the reticuloendothelial system (RES) located in the liver and spleen, and pass through the renal filtration, similar to our previous report associated with PEGylated Au DENPs.[13]

Histological Evaluation of Organ Toxicity. The long-term toxicity of PEGylated Au PENPs was assessed by monitoring the pathological changes of several major organs of the mice including heart, liver, spleen, lung, and kidney at one month post intravenous injection of the $[(Au^0)_{200}$-PEI·NHAc-*m*PEG] NPs ([Au] = 0.1 M, 100 μL in PBS). H&E staining of the major organs shows that compared to the control mice treated with PBS, the injection of the PEGylated Au PENPs does not seem to induce any significant changes in the morphology of the organ sections (Figure 8). Our results imply that the PEGylated Au PENPs display good organ compatibility, which is very important for their further in vivo biomedical applications.

CONCLUSION

To conclude, we developed a facile approach to fabricating PEGylated Au PENPs for in vivo blood pool and tumor CT imaging applications. The partial PEGylation of PEI surface amines enabled the use of PEGylated PEI as a template for effective AuNP synthesis. By varying the molar feeding ratio of the Au salt/PEI-*m*PEG, PEGylated Au PENPs with an Au core size of 1.9−4.6 nm can be formed. The prepared PEGylated Au PENPs are water dispersible, colloidally stable, and non-cytotoxic in the given concentration range. With the sufficiently long blood retention time, as confirmed by pharmacokinetics studies, and better X-ray attenuation property than iodinated small molecular CT contrast agents (e.g., Omnipaque), the developed PEGylated Au PENPs are able to be used as a contrast agent not only for blood pool CT imaging, but also for tumor CT imaging via a passive EPR effect. With the proven long-term organ compatibility, the developed PEGylated Au PENPs may hold great promise to be used as a versatile contrast agent for different CT imaging applications. The significance of this study is that, rather than the use of expensive dendrimers, cost-effective branched PEI may be developed as a multifunctional platform through appropriate surface functionalization for various theranostic applications.

ASSOCIATED CONTENT

Supporting Information

Additional DLS; ^{1}H NMR; MALDI-TOF mass spectroscopy; TEM; high-resolution TEM, SAED, EDS, and TGA characterization data; stability assessment of $[(Au^0)_n$−PEI·$NH_2]$, $[(Au^0)_n$−PEI·NHAc], and $[(Au^0)_n$−PEI·NHAc-*m*PEG] NPs; additional hemolysis assay; and KB cell morphology observation data. This material is available free of charge via the Internet at http://pubs.acs.org.

AUTHOR INFORMATION

Corresponding Authors

*E-mail: mingwu_shen@yahoo.com.
*E-mail: guixiangzhang@sina.com.
*E-mail: xshi@dhu.edu.cn.

Author Contributions

$^{\|}$These authors contributed equally to this work.

Notes

The authors declare no competing financial interest.

ACKNOWLEDGMENTS

This research is financially supported by the National Natural Science Foundation of China (81351050, 81101150, 21273032, and 81271384), the Fund of the Science and Technology Commission of Shanghai Municipality (11nm0506400 and 12520705500), the Ph.D. Programs Foundation of the Ministry of Education of China (20130075110004), and the Program for Professor of Special Appointment (Eastern Scholar) at Shanghai Institutions of Higher Learning. B.Z. thanks the Innovation Funds of Donghua University Doctorate Dissertation of Excellence (CUSF-DH-D-2014034). C.P. thanks the support from the Shanghai Natural Science Foundation (14ZR1432400).

REFERENCES

(1) Boyer, D.; Tamarat, P.; Maali, A.; Lounis, B.; Orrit, M. Photothermal Imaging of Nanometer-Sized Metal Particles among Scatterers. *Science* **2002**, *297*, 1160−1163.

(2) Huang, X.; El-Sayed, I. H.; Qian, W.; El-Sayed, M. A. Cancer Cells Assemble and Align Gold Nanorods Conjugated to Antibodies to Produce Highly Enhanced, Sharp, and Polarized Surface Raman Spectra: A Potential Cancer Diagnostic Marker. *Nano Lett.* **2007**, *7*, 1591−1597.

(3) Chen, T.-J.; Cheng, T.-H.; Chen, C.-Y.; Hsu, S. C. N.; Cheng, T.-L.; Liu, G.-C.; Wang, Y.-M. Targeted Herceptin-Dextran Iron Oxide Nanoparticles for Noninvasive Imaging of HER2/Neu Receptors Using MRI. *J. Biol. Inorg. Chem.* **2009**, *14*, 253−260.
(4) Åkerman, M. E.; Chan, W. C.; Laakkonen, P.; Bhatia, S. N.; Ruoslahti, E. Nanocrystal Targeting in Vivo. *Proc. Natl. Acad. Sci. U.S.A.* **2002**, *99*, 12617−12621.
(5) Ji, X.; Song, X.; Li, J.; Bai, Y.; Yang, W.; Peng, X. Size Control of Gold Nanocrystals in Citrate Reduction: The Third Role of Citrate. *J. Am. Chem. Soc.* **2007**, *129*, 13939−13948.
(6) Kim, J.; Piao, Y.; Hyeon, T. Multifunctional Nanostructured Materials for Multimodal Imaging, and Simultaneous Imaging and Therapy. *Chem. Soc. Rev.* **2009**, *38*, 372−390.
(7) Peng, C.; Li, K.; Cao, X.; Xiao, T.; Hon, W.; Zheng, L.; Guo, R.; Shen, M.; Zhang, G.; Shi, X. Facile Formation of Dendrimer-Stabilized Gold Nanoparticles Modified with Diatrizoic Acid for Enhanced Computed Tomography Imaging Applications. *Nanoscale* **2012**, *4*, 6768−6778.
(8) Kim, J.; Park, S.; Lee, J. E.; Jin, S. M.; Lee, J. H.; Lee, I. S.; Yang, I.; Kim, J.-S.; Kim, S. K.; Cho, M.-H.; Hyeon, T. Designed Fabrication of Multifunctional Magnetic Gold Nanoshells and Their Application to Magnetic Resonance Imaging and Photothermal Therapy. *Angew. Chem., Int. Ed.* **2006**, *45*, 7754−7758.
(9) Debouttiere, P. J.; Roux, S.; Vocanson, F.; Billotey, C.; Beuf, O.; Favre-Reguillon, A.; Lin, Y.; Pellet-Rostaing, S.; Lamartine, R.; Perriat, P.; Tillement, O. Design of Gold Nanoparticles for Magnetic Resonance Imaging. *Adv. Funct. Mater.* **2006**, *16*, 2330−2339.
(10) Wijaya, A.; Schaffer, S. B.; Pallares, I. G.; Hamad-Schifferli, K. Selective Release of Multiple DNA Oligonucleotides from Gold Nanorods. *ACS Nano* **2009**, *3*, 80−86.
(11) Chen, Q.; Li, K.; Wen, S.; Liu, H.; Peng, C.; Cai, H.; Shen, M.; Zhang, G.; Shi, X. Targeted CT/MR Dual Mode Imaging of Tumors Using Multifunctional Dendrimer-Entrapped Gold Nanoparticles. *Biomaterials* **2013**, *34*, 5200−5209.
(12) Nam, T.; Park, S.; Lee, S.-Y.; Park, K.; Choi, K.; Song, I. C.; Han, M. H.; Leary, J. J.; Yuk, S. A.; Kwon, I. C.; Kim, K.; Jeong, S. Y. Tumor Targeting Chitosan Nanoparticles for Dual-Modality Optical/MR Cancer Imaging. *Bioconjugate Chem.* **2010**, *21*, 578−582.
(13) Wen, S.; Li, K.; Cai, H.; Chen, Q.; Shen, M.; Huang, Y.; Peng, C.; Hou, W.; Zhu, M.; Zhang, G.; Shi, X. Multifunctional Dendrimer-Entrapped Gold Nanoparticles for Dual Mode CT/MR Imaging Applications. *Biomaterials* **2013**, *34*, 1570−1580.
(14) Michalet, X.; Pinaud, F. F.; Bentolila, L. A.; Tsay, J. M.; Doose, S.; Li, J. J.; Sundaresan, G.; Wu, A. M.; Gambhir, S. S.; Weiss, S. Quantum Dots for Live Cells, in Vivo Imaging, and Diagnostics. *Science* **2005**, *307*, 538−544.
(15) Gao, X. H.; Yang, L. L.; Petros, J. A.; Marshal, F. F.; Simons, J. W.; Nie, S. M. In Vivo Molecular and Cellular Imaging with Quantum Dots. *Curr. Opin. Biotechnol.* **2005**, *16*, 63−72.
(16) Biju, V.; Itoh, T.; Anas, A.; Sujith, A.; Ishikawa, M. Semiconductor Quantum Dots and Metal Nanoparticles: Syntheses, Optical Properties, and Biological Applications. *Anal. Bioanal. Chem.* **2008**, *391*, 2469−2495.
(17) Larson, D. R.; Zipfel, W. R.; Williams, R. M.; Clark, S. W.; Bruchez, M. P.; Wise, F. W.; Webb, W. W. Water-Soluble Quantum Dots for Multiphoton Fluorescence Imaging in Vivo. *Science* **2003**, *300*, 1434−1436.
(18) Oh, M. H.; Lee, N.; Kim, H.; Park, S. P.; Piao, Y.; Lee, J.; Jun, S. W.; Moon, W. K.; Choi, S. H.; Hyeon, T. Large-Scale Synthesis of Bioinert Tantalum Oxide Nanoparticles for X-Ray Computed Tomography Imaging and Bimodal Image-Guided Sentinel Lymph Node Mapping. *J. Am. Chem. Soc.* **2011**, *133*, 5508−5515.
(19) Cai, Q.-Y.; Kim, S. H.; Choi, K. S.; Kim, S. Y.; Byun, S. J.; Kim, K. W.; Park, S. H.; Juhng, S. K.; Yoon, K.-H. Colloidal Gold Nanoparticles as a Blood-Pool Contrast Agent for X-Ray Computed Tomography in Mice. *Invest. Radiol.* **2007**, *42*, 797−806.
(20) Kim, D.; Park, S.; Lee, J. H.; Jeong, Y. Y.; Jon, S. Antibiofouling Polymer-Coated Gold Nanoparticles as a Contrast Agent for in Vivo X-Ray Computed Tomography Imaging. *J. Am. Chem. Soc.* **2007**, *129*, 7661−7665.
(21) Fang, Y.; Peng, C.; Guo, R.; Zheng, L.; Qin, J.; Zhou, B.; Shen, M.; Lu, X.; Zhang, G.; Shi, X. Dendrimer-Stabilized Bismuth Sulfide Nanoparticles: Synthesis, Characterization, and Potential Computed Tomography Imaging Applications. *Analyst* **2013**, *138*, 3172−3180.
(22) Schwenzer, N. F.; Springer, F.; Schraml, C.; Stefan, N.; Machann, J.; Schick, F. Non-Invasive Assessment and Quantification of Liver Steatosis by Ultrasound, Computed Tomography and Magnetic Resonance. *J. Hepatol.* **2009**, *51*, 433−445.
(23) deKrafft, K. E.; Xie, Z.; Cao, G.; Tran, S.; Ma, L.; Zhou, O. Z.; Lin, W. Iodinated Nanoscale Coordination Polymers as Potential Contrast Agents for Computed Tomography. *Angew. Chem., Int. Ed.* **2009**, *48*, 9901−9904.
(24) Haller, C.; Hizoh, I. The Cytotoxicity of Iodinated Radiocontrast Agents on Renal Cells in Vitro. *Invest. Radiol.* **2004**, *39*, 149−154.
(25) Yordanov, A. T.; Lodder, A. L.; Woller, E. K.; Cloninger, M. J.; Patronas, N.; Milenic, D.; Brechbiel, M. W. Novel Iodinated Dendritic Nanoparticles for Computed Tomography (CT) Imaging. *Nano Lett.* **2002**, *2*, 595−599.
(26) Hallouard, F.; Anton, N.; Choquet, P.; Constantinesco, A.; Vandamme, T. Iodinated Blood Pool Contrast Media for Preclinical X-Ray Imaging Applications—A Review. *Biomaterials* **2010**, *31*, 6249−6268.
(27) Alric, C.; Taleb, J.; Le Duc, G.; Mandon, C.; Billotey, C.; Le Meur-Herland, A.; Brochard, T.; Vocanson, F.; Janier, M.; Perriat, P.; Roux, S.; Tillement, O. Gadolinium Chelate Coated Gold Nanoparticles as Contrast Agents for Both X-Ray Computed Tomography and Magnetic Resonance Imaging. *J. Am. Chem. Soc.* **2008**, *130*, 5908−5915.
(28) Li, D.; He, Q.; Cui, Y.; Wang, K.; Zhang, X.; Li, J. Thermosensitive Copolymer Networks Modify Gold Nanoparticles for Nanocomposite Entrapment. *Chem.—Eur. J.* **2007**, *13*, 2224−2229.
(29) Li, D.; Cui, Y.; Wang, K.; He, Q.; Yan, X.; Li, J. Thermosensitive Nanostructures Comprising Gold Nanoparticles Grafted with Block Copolymers. *Adv. Funct. Mater.* **2007**, *17*, 3134−3140.
(30) Li, D.; He, Q.; Cui, Y.; Li, J. Fabrication of pH-Responsive Nanocomposites of Gold Nanoparticles/Poly(4-vinylpyridine). *Chem. Mater.* **2007**, *19*, 412−417.
(31) Li, D.; He, Q.; Li, J. Smart Core/Shell Nanocomposites: Intelligent Polymers Modified Gold Nanoparticles. *Adv. Colloid Interface Sci.* **2009**, *149*, 28−38.
(32) Li, D.; He, Q.; Yang, Y.; Mohwald, H.; Li, J. Two-Stage pH Response of Poly(4-vinylpyridine) Grafted Gold Nanoparticles. *Macromolecules* **2008**, *41*, 7254−7256.
(33) Guo, R.; Wang, H.; Peng, C.; Shen, M.; Zheng, L.; Zhang, G.; Shi, X. Enhanced X-Ray Attenuation Property of Dendrimer-Entrapped Gold Nanoparticles Complexed with Diatrizoic Acid. *J. Mater. Chem.* **2011**, *21*, 5120−5127.
(34) Guo, R.; Wang, H.; Peng, C.; Shen, M. W.; Pan, M. J.; Cao, X. Y.; Zhang, G. X.; Shi, X. Y. X-Ray Attenuation Property of Dendrimer-Entrapped Gold Nanoparticles. *J. Phys. Chem. C* **2010**, *114*, 50−56.
(35) Liu, H.; Shen, M.; Zhao, J.; Guo, R.; Cao, X.; Zhang, G.; Shi, X. Tunable Synthesis and Acetylation of Dendrimer-Entrapped or Dendrimer-Stabilized Gold-Silver Alloy Nanoparticles. *Colloids Surf., B* **2012**, *94*, 58−67.
(36) Liu, H.; Wang, H.; Xu, Y.; Guo, R.; Wen, S.; Huang, Y.; Liu, W.; Shen, M.; Zhao, J.; Zhang, G.; Shi, X. Lactobionic Acid-Modified Dendrimer-Entrapped Gold Nanoparticles for Targeted Computed Tomography Imaging of Human Hepatocellular Carcinoma. *ACS Appl. Mater. Interfaces* **2014**, *6*, 6944−6953.
(37) Liu, H.; Wang, H.; Xu, Y.; Shen, M.; Zhao, J.; Zhang, G.; Shi, X. Synthesis of PEGylated Low Generation Dendrimer-Entrapped Gold Nanoparticles for CT Imaging Applications. *Nanoscale* **2014**, *6*, 4521−4526.
(38) Liu, H.; Xu, Y.; Wen, S.; Chen, Q.; Zheng, L.; Shen, M.; Zhao, J.; Zhang, G.; Shi, X. Targeted Tumor Computed Tomography

Imaging Using Low-Generation Dendrimer-Stabilized Gold Nanoparticles. *Chem.—Eur. J.* **2013**, *19*, 6409−6416.
(39) Liu, H.; Xu, Y.; Wen, S.; Zhu, J.; Zheng, L.; Shen, M.; Zhao, J.; Zhang, G.; Shi, X. Facile Formation of Low Generation Dendrimer-Stabilized Gold Nanoparticles for in Vivo X-Ray Computed Tomography Imaging Applications. *Polym. Chem.* **2013**, *4*, 1788−1795.
(40) Peng, C.; Qin, J.; Zhou, B.; Chen, Q.; Shen, M.; Zhu, M.; Lu, X.; Shi, X. Targeted Tumor CT Imaging Using Folic Acid-Modified PEGylated Dendrimer-Entrapped Gold Nanoparticles. *Polym. Chem.* **2013**, *4*, 4412−4424.
(41) Peng, C.; Zheng, L.; Chen, Q.; Shen, M.; Guo, R.; Wang, H.; Cao, X.; Zhang, G.; Shi, X. PEGylated Dendrimer-Entrapped Gold Nanoparticles for in Vivo Blood Pool and Tumor Imaging by Computed Tomography. *Biomaterials* **2012**, *33*, 1107−1119.
(42) Wang, H.; Zheng, L.; Peng, C.; Guo, R.; Shen, M.; Shi, X.; Zhang, G. Computed Tomography Imaging of Cancer Cells Using Acetylated Dendrimer-Entrapped Gold Nanoparticles. *Biomaterials* **2011**, *32*, 2979−2988.
(43) Wang, H.; Zheng, L.; Peng, C.; Shen, M.; Shi, X.; Zhang, G. Folic Acid-Modified Dendrimer-Entrapped Gold Nanoparticles as Nanoprobes for Targeted CT Imaging of Human Lung Adenocarcinoma. *Biomaterials* **2013**, *34*, 470−480.
(44) Kojima, C.; Umeda, Y.; Ogawa, M.; Harada, A.; Magata, Y.; Kono, K. X-Ray Computed Tomography Contrast Agents Prepared by Seeded Growth of Gold Nanoparticles in PEGylated Dendrimer. *Nanotechnology* **2010**, *21*, 245104.
(45) Appelhans, D.; Komber, H.; Quadir, M. A.; Richter, S.; Schwarz, S.; van der Vlist, J.; Aigner, A.; Mueller, M.; Loos, K.; Seidel, J.; Arndt, K.-F.; Haag, R.; Voit, B. Hyperbranched PEI with Various Oligosaccharide Architectures: Synthesis, Characterization, ATP Complexation, and Cellular Uptake Properties. *Biomacromolecules* **2009**, *10*, 1114−1124.
(46) Elfinger, M.; Pfeifer, C.; Uezguen, S.; Golas, M. M.; Sander, B.; Maucksch, C.; Stark, H.; Aneja, M. K.; Rudolph, C. Self-Assembly of Ternary Insulin-Polyethylenimine (PEI)-DNA Nanoparticles for Enhanced Gene Delivery and Expression in Alveolar Epithelial Cells. *Biomacromolecules* **2009**, *10*, 2912−2920.
(47) Hoebel, S.; Loos, A.; Appelhans, D.; Schwarz, S.; Seidel, J.; Voit, B.; Aigner, A. Maltose- and Maltotriose-Modified, Hyperbranched Poly(ethylene imine)s (OM-PEIs): Physicochemical and Biological Properties of DNA and SiRNA Complexes. *J. Controlled Release* **2011**, *149*, 146−158.
(48) Liang, S.; Yu, H.; Xiang, J.; Yang, W.; Chen, X.; Liu, Y.; Gao, C.; Yan, G. New Naphthalimide Modified Polyethylenimine Nanoparticles as Fluorescent Probe for DNA Detection. *Spectrochim. Acta, Part A* **2012**, *97*, 359−365.
(49) Tomalia, D. A., Frechet, J. M. J., Eds. *Dendrimers and Other Dendritic Polymers*. John Wiley & Sons, Ltd.: New York, 2001.
(50) Wen, S.; Zheng, F.; Shen, M.; Shi, X. Surface Modification and PEGylation of Branched Polyethyleneimine for Improved Biocompatibility. *J. Appl. Polym. Sci.* **2013**, *128*, 3807−3813.
(51) Thomas, M.; Klibanov, A. M. Conjugation to Gold Nanoparticles Enhances Polyethylenimine's Transfer of Plasmid DNA into Mammalian Cells. *Proc. Natl. Acad. Sci. U.S.A.* **2003**, *100*, 9138−9143.
(52) Koeth, A.; Appelhans, D.; Prietzel, C.; Koetz, J. Asymmetric Gold Nanoparticles Synthesized in the Presence of Maltose-Modified Poly(ethyleneimine). *Colloids Surf., A* **2012**, *414*, 50−56.
(53) Koeth, A.; Tiersch, B.; Appelhans, D.; Gradzielski, M.; Coelfen, H.; Koetz, J. Synthesis of Core-Shell Gold Nanoparticles with Maltose-Modified Poly(ethyleneimine). *J. Dispersion Sci. Technol.* **2012**, *33*, 52−60.
(54) Tong, W.; Cao, X.; Wen, S.; Guo, R.; Shen, M.; Wang, J.; Shi, X. Enhancing the Specificity and Efficiency of Polymerase Chain Reaction Using Polyethyleneimine-Based Derivatives and Hybrid Nanocomposites. *Int. J. Nanomed.* **2012**, *7*, 1069−1078.
(55) Wen, S.; Zheng, F.; Shen, M.; Shi, X. Synthesis of Polyethyleneimine-Stabilized Gold Nanoparticles for Colorimetric Sensing of Heparin. *Colloids Surf., A* **2013**, *419*, 80−86.
(56) Li, J.; Zheng, L.; Cai, H.; Sun, W.; Shen, M.; Zhang, G.; Shi, X. Facile One-Pot Synthesis of Fe_3O_4@Au Composite Nanoparticles for Dual-Mode MR/CT Imaging Applications. *ACS Appl. Mater. Interfaces* **2013**, *5*, 10357−10366.
(57) Shi, X.; Lee, I.; Baker, J. R., Jr. Acetylation of Dendrimer-Entrapped Gold and Silver Nanoparticles. *J. Mater. Chem.* **2008**, *18*, 586−593.
(58) Majoros, I. J.; Keszler, B.; Woehler, S.; Bull, T.; Baker, J. R. Acetylation of Poly(amidoamine) Dendrimers. *Macromolecules* **2003**, *36*, 5526−5529.
(59) Wen, S.; Zhao, Q.; An, X.; Zhu, J.; Hou, W.; Li, K.; Huang, Y.; Shen, M.; Zhu, W.; Shi, X. Multifunctional PEGylated Multiwalled Carbon Nanotubes for Enhanced Blood Pool and Tumor MR Imaging. *Adv. Healthcare Mater.* **2014**, DOI: 10.1002/adhm.201300631.
(60) Ghosh, S. K.; Pal, T. Interparticle Coupling Effect on the Surface Plasmon Resonance of Gold Nanoparticles: From Theory to Applications. *Chem. Rev.* **2007**, *107*, 4797−4862.
(61) Shi, X.; Sun, K.; Baker, J. R., Jr. Spontaneous Formation of Functionalized Dendrimer-Stabilized Gold Nanoparticles. *J. Phys. Chem. C* **2008**, *112*, 8251−8258.
(62) Huang, X.; Peng, X.; Wang, Y.; Wang, Y.; Shin, D. M.; El-Sayed, M. A.; Nie, S. A Reexamination of Active and Passive Tumor Targeting by Using Rod-Shaped Gold Nanocrystals and Covalently Conjugated Peptide Ligands. *ACS Nano* **2010**, *4*, 5887−5896.
(63) Maeda, H. Tumor-Selective Delivery of Macromolecular Drugs via the EPR Effect: Background and Future Prospects. *Bioconjugate Chem.* **2010**, *21*, 797−802.
(64) Fang, J.; Nakamura, H.; Maeda, H. The EPR Effect: Unique Features of Tumor Blood Vessels for Drug Delivery, Factors Involved, and Limitations and Augmentation of the Effect. *Adv. Drug Delivery Rev.* **2011**, *63*, 136−151.